

The quantum cascade laser as a self-pumped parametric oscillator

(Supplemental Information)

Tobias S. Mansuripur,¹ Camille Vernet,^{2,3} Paul Chevalier,² Guillaume Aoust,^{2,4} Benedikt Schwarz,^{2,5} Feng Xie,⁶ Catherine Caneau,⁷ Kevin Lascola,⁶ Chung-en Zah,⁶ David P. Caffey,⁸ Timothy Day,⁸ Leo J. Missaggia,⁹ Michael K. Connors,⁹ Christine Wang,⁹ Alexey Belyanin,¹⁰ and Federico Capasso^{2,*}

¹*Department of Physics, Harvard University, Cambridge, MA 02138 USA*

²*John A. Paulson School of Engineering and Applied Sciences,
Harvard University, Cambridge, MA 02138 USA*

³*Ecole Polytechnique, Palaiseau, France*

⁴*ONERA, The French Aerospace Lab, 91123 Palaiseau, France*

⁵*Institute of Solid State Electronics, TU Wien, Vienna 1040, Austria*

⁶*Thorlabs Quantum Electronics (TQE), Jessup, Maryland 20794 USA*

⁷*Corning, Inc., Corning, NY 14831 USA*

⁸*Daylight Solutions, Inc., San Diego, CA 92128 USA*

⁹*Massachusetts Institute of Technology,
Lincoln Laboratory, Lexington, MA 02420 USA*

¹⁰*Department of Physics and Astronomy,
Texas A & M University, College Station, Texas 77843 USA*

* capasso@seas.harvard.edu

I. COMMENTS ON POWER VS. CURRENT CURVES

In the single-mode regime, the intracavity intensity of the single-mode determines the strength of the parametric interaction with the sidebands. Therefore, we would like to calculate the intracavity intensity from the measured output power. We remain true to the distributed loss approximation, for which the output power is given by

$$P_{out} = \frac{\alpha_m \langle E^2 \rangle L w h}{\sqrt{\mu/\epsilon}} \quad (1)$$

where $\alpha_m = \ln[1/(R_1 R_2)]/(2L)$, the length, width, and height of the cavity are L , w , and h , and the time-average intensity of the single-mode is $\langle E^2 \rangle = 2|\mathcal{E}_0|^2$. We are assuming a uniform field intensity in the transverse dimensions, and therefore not worrying about the transverse overlap factor. We can rearrange this equation for the intracavity intensity

$$|\tilde{\mathcal{E}}_0|^2 \equiv \kappa^2 T_1 T_2 |\mathcal{E}_0|^2 = \frac{2d^2 T_1 T_2 \sqrt{\mu_0/\epsilon_0}}{\hbar^2 n_{\text{eff}} \alpha_m L w h} P_{out}. \quad (2)$$

With this equation, we can convert the measured total output power of each laser into the intracavity intensity, using our measured values of the refractive index n_{eff} and the dephasing time T_2 , our best estimates for d and T_1 , and in the case of the HR/AR laser we have used $R_1 = 1$, $R_2 = 0.01$. The result is plotted in Fig. S1 as a function of J/J_{th} , which is the same as the inset in Fig. 1 of the main text.

The theoretical formula for the intracavity intensity is

$$|\tilde{\mathcal{E}}_0|^2 = \frac{p - 1}{1 + \gamma_D/2}, \quad (3)$$

where $p \equiv w_{eq}/w_{th}$ is the pump parameter. We emphasize that p is not the same as J/J_{th} . The slope of $|\tilde{\mathcal{E}}_0|^2$ vs. p is always between 2/3 and 1, depending on the diffusion parameter γ_D . The reference line in Fig. S1 is drawn with a slope of one to indicate that each of the $|\tilde{\mathcal{E}}_0|^2$ vs. J/J_{th} curves has a slope greater than one. Therefore, we conclude that J/J_{th} must underestimate p . One factor that contributes to this underestimation is the transparency current J_{trans} : a fixed amount of current that must be delivered to the active region simply to raise the inversion from a negative number to zero. To understand this simply, suppose that the equilibrium inversion scales like $w_{eq} \propto J - J_{\text{trans}}$, and that J_{trans} remains a constant number at threshold and above. Then the pump parameter $p \equiv w_{eq}/w_{th}$ is expressed in terms of J as

$$p = \frac{J - J_{\text{trans}}}{J_{\text{th}} - J_{\text{trans}}}. \quad (4)$$

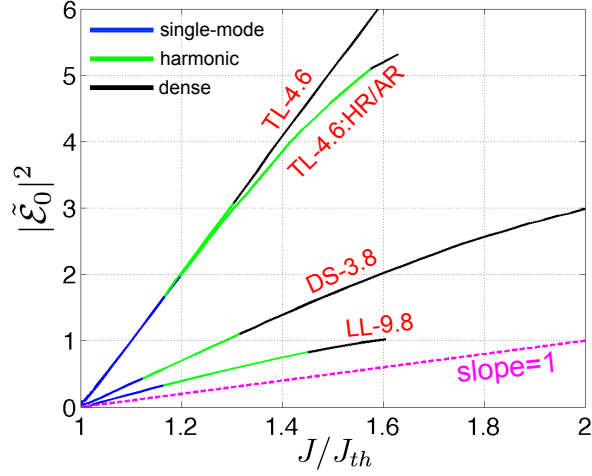


FIG. S1. The measured output power of each QCL (from both facets) is converted to the intracavity intensity $|\tilde{\xi}_0|^2$, and plotted against J/J_{th} . Each curve is color-coded to indicate the range over which the laser operates in a single-mode, harmonic state, or dense state. Note that the quantity $|\tilde{\xi}_0|^2$ is only meaningful in the single-mode regime, because we are interested in the intensity of the single-mode before the harmonic regime sets in. A line with a slope of one is drawn as a reference.

For example, suppose that for a laser with $J_{th} = 500$ mA the harmonic state kicks in at 550 mA, or $J/J_{th} = 1.1$. If the transparency current was $J_{trans} = 250$ mA, (in other words, half of the threshold current, which is reasonable for QCLs), then the pump parameter at the harmonic state onset would be $p = (550 - 250)/(500 - 250) = 1.2$. Thus, J/J_{th} underestimates p .

A more rigorous study is required to determine J_{trans} for each laser, which can be done by measuring many lasers of the same active region but different lengths. Once J_{trans} is known, the slope of $|\tilde{\xi}_0|^2$ vs. p should fall between $2/3$ and 1 and in principle a value for γ_D can be extracted, allowing one to quantify the amount of diffusion present.

II. HYSTERESIS OF IV CURVE

The IV curve of device DS-3.8 shown in Fig. S2 demonstrates a hysteresis. When starting below threshold and increasing the current (red), the voltage of the laser decreases (negative differential resistance) when the noisy harmonic state transitions to the dense state at 523 mA. (In the spectra shown in Fig. 3(c) of the manuscript, this transition occurs at 502 mA.

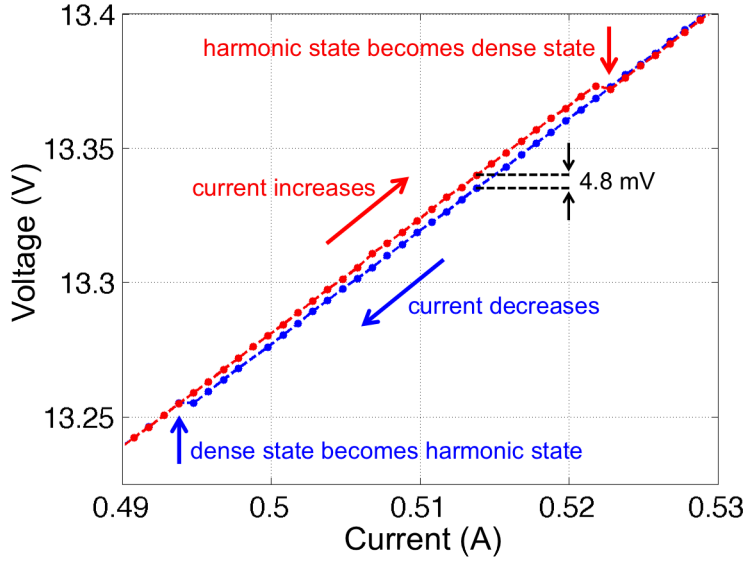


FIG. S2. The IV curve of DS-3.8 exhibits a hysteresis as the current is increased (red) and decreased (blue). The hysteresis is correlated with the transition from the noisy harmonic state to the dense state.

The exact current at which the transition occurs is not identical from one experiment to another, but occurs predictably within a range of about 20 mA.) Once the laser reaches the dense state and the current is subsequently decreased (blue), the laser persists in the dense state at currents below 523 mA. This is responsible for the hysteresis loop. For the same current, the voltage is 4.8 mV smaller when in the dense state than in the noisy harmonic state. At 494 mA, the dense state transitions to the noisy harmonic state, and the two voltage curves overlap again.

The lower voltage of the dense state indicates a larger radiative photocurrent, which implies that the output power of the laser is slightly larger in the dense state than in the harmonic state, for the same current pumping. (While we could have measured the output power to demonstrate this, the IV measurement is more sensitive.) Thus, the dense state is more efficient at extracting photons from upper state electrons and is, in one sense, more stable. Therefore, once the laser enters the dense state, it likes to remain there even as the current is decreased.

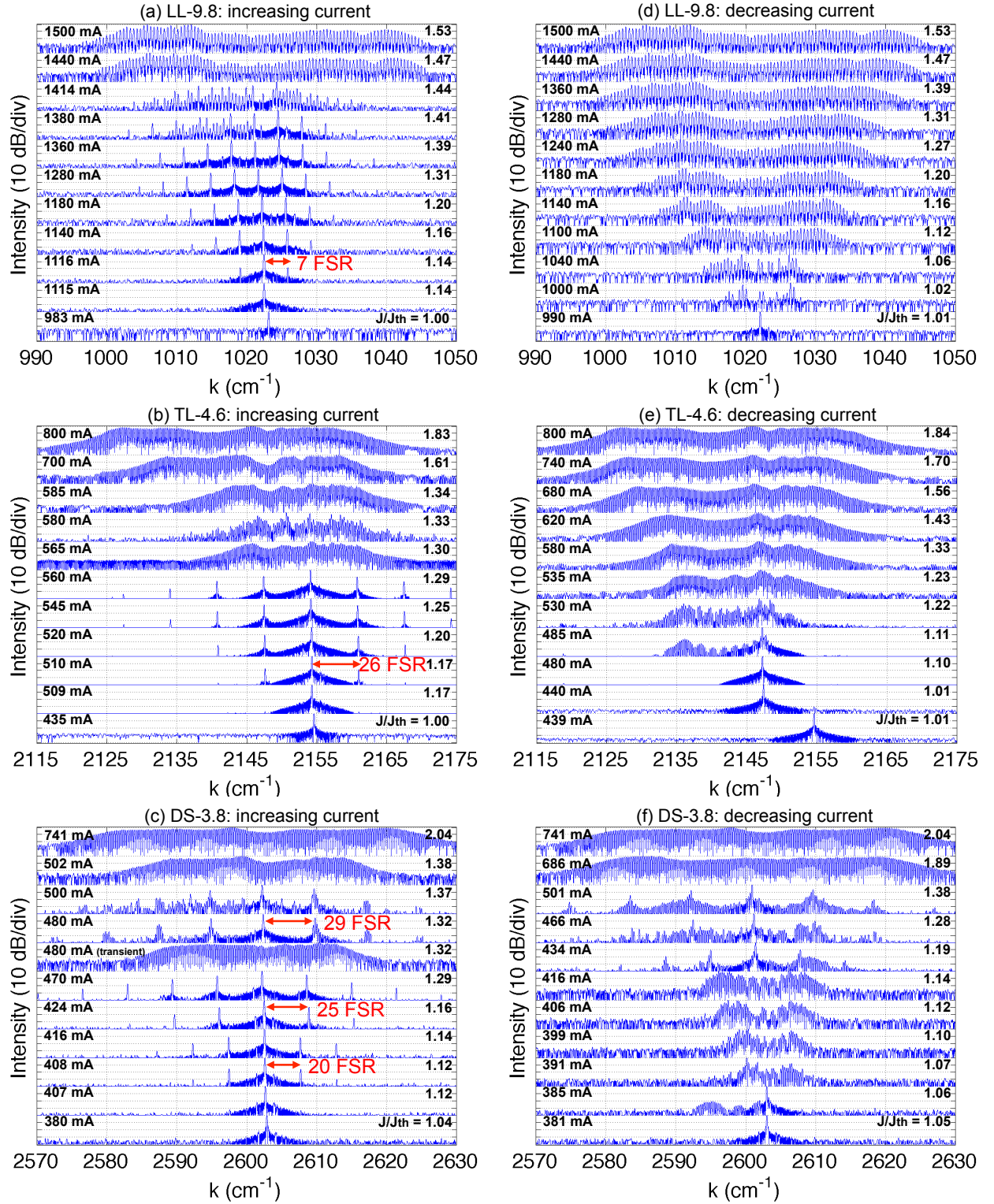


FIG. S3. The spectra of the three uncoated devices as the current is ramped up and as it is ramped down. Of the six plots, only (e) and (f) were not included in the main text.

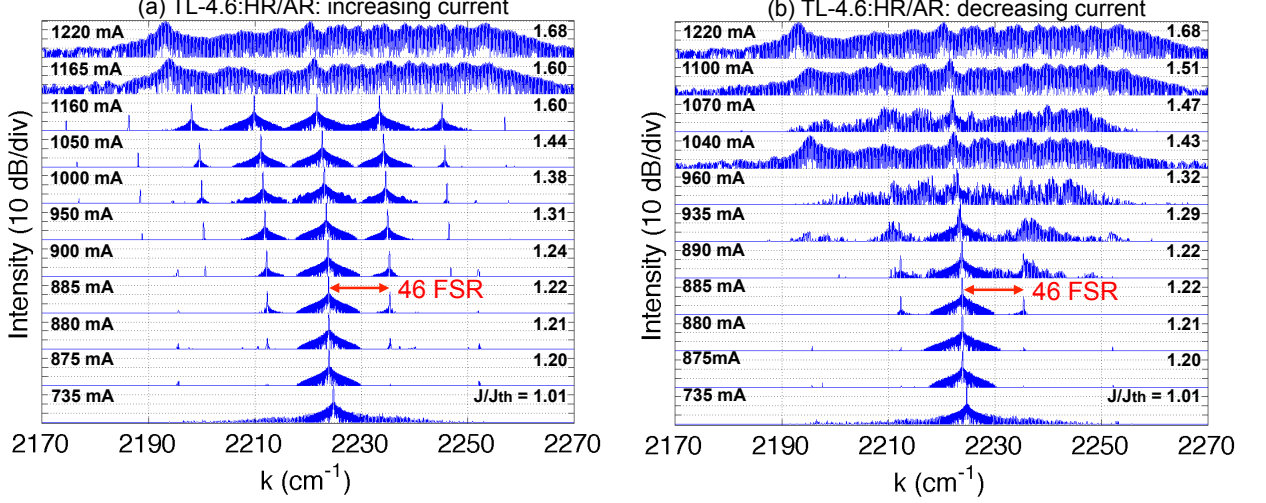


FIG. S4. The spectra of TL-4.6:HR/AR as the current is (a) ramped up and (b) ramped down. Only plot (b) was not presented in the main text.

III. ADDITIONAL DATA ON SPECTRAL HYSTERESIS

In Fig. S3, the spectra of the three uncoated devices are plotted as the current is increased starting from below threshold, and also as the current is decreased. For devices LL-9.8 and TL-4.6, once the dense state is reached it persists as the current is decreased until the single-mode state reappears. Device DS-3.8 also exhibits noisy harmonic states as the current is decreased. For all three devices, it is true that the clean harmonic state never reappears once the laser has reached the dense state.

In Fig. S4, the spectra of TL-4.6:HR/AR are plotted as the current is increased and then decreased. As the current is decreased, the dense state persists until a noisy harmonic state appears at $1.29J_{\text{th}}$. Interestingly, in this device—unlike the uncoated ones—the clean harmonic state with one pair of sidebands reappears at 885 mA, which is quite close to the instability threshold of 880 mA found when the current is ramped upwards. The reappearance of the harmonic state may also suggest that the sidebands are in the parametric enhancement regime, in addition to the two pieces of evidence discussed in the main text; namely, the large sideband spacing (46 FSR) and the large range of intracavity power over which the harmonic state persists.

IV. THEORY: SINGLE-MODE SOLUTION

This section gives a more detailed derivation of the single-mode solution, including the intracavity power as a function of pumping, and the population inversion as a function of position and pumping.

For a two level system with upper state $|a\rangle$ and lower state $|b\rangle$, the material equations in the non-rotating frame and the field equation are

$$\frac{d\rho_{ab}}{dt} = -i\omega_{ba}\rho_{ab} - \frac{id}{\hbar}E(t)w - \frac{\rho_{ab}}{T_2} \quad (5)$$

$$\frac{dw}{dt} = \frac{-2id}{\hbar}E(t)(\rho_{ab} - \rho_{ab}^*) + \frac{w_{eq} - w}{T_1} + D\frac{\partial^2 w}{\partial z^2} \quad (6)$$

$$\frac{\partial^2 E}{\partial z^2} - \frac{1}{c^2} \frac{\partial^2 E}{\partial t^2} = Nd\mu \frac{\partial^2}{\partial t^2}(\rho_{ab} + \rho_{ab}^*). \quad (7)$$

We emphasize that these equations are in the non-rotating frame, whereas the equations we have used in the main text [1] were already in the rotating frame and the RWA had already been applied. However, since we are here dealing with two counter-propagating waves, we chose to more closely follow the approach in [2]. We make the following ansatzes:

$$E(z, t) = \frac{1}{\sqrt{2}} [\mathcal{E}_R(z, t)e^{-i(\omega t - kz)} + \mathcal{E}_L(z, t)e^{-i(\omega t + kz)} + c.c.] \quad (8)$$

$$\rho_{ab}(z, t) = \eta_R^*(z, t)e^{-i(\omega t - kz)} + \eta_L^*(z, t)e^{-i(\omega t + kz)} \quad (9)$$

$$w(z, t) = w_{\text{DC}}(z, t) + w_2(z, t)e^{i2kz} + w_2^*(z, t)e^{-i2kz}. \quad (10)$$

(We use the subscript “DC” rather than “0” for the spatial average of the population inversion, w_{DC} , because the subscript 0 is used throughout the text to refer to the primary mode. No such ambiguity occurs for the subscript “2.”) Plugging the ansatzes into the differential equations, and making the RWA as well as the slowly-varying envelope approximation

(SVEA) yields the following equations:

$$\frac{d\eta_R^*}{dt} = \frac{-i\kappa}{2\sqrt{2}}(\mathcal{E}_R w_{\text{DC}} + \mathcal{E}_L w_2) - \left(\frac{1}{T_2} + i\Delta\right)\eta_R^* \quad (11)$$

$$\frac{d\eta_L^*}{dt} = \frac{-i\kappa}{2\sqrt{2}}(\mathcal{E}_L w_{\text{DC}} + \mathcal{E}_R w_2^*) - \left(\frac{1}{T_2} + i\Delta\right)\eta_L^* \quad (12)$$

$$\frac{dw_{\text{DC}}}{dt} = \frac{i\kappa}{\sqrt{2}}(\mathcal{E}_R \eta_R + \mathcal{E}_L \eta_L - c.c.) + \frac{w_{eq} - w_{\text{DC}}}{T_1} \quad (13)$$

$$\frac{dw_2}{dt} = \frac{i\kappa}{\sqrt{2}}(\mathcal{E}_R \eta_L - \mathcal{E}_L^* \eta_R^*) - \frac{w_2}{T_1} - 4k^2 D w_2 \quad (14)$$

$$\frac{1}{c} \frac{\partial \mathcal{E}_R}{\partial t} = -\frac{\partial \mathcal{E}_R}{\partial z} + \frac{i\sqrt{2}\alpha}{\kappa T_2} \eta_R^* - \frac{\ell_0}{2} \mathcal{E}_R \quad (15)$$

$$\frac{1}{c} \frac{\partial \mathcal{E}_L}{\partial t} = +\frac{\partial \mathcal{E}_L}{\partial z} + \frac{i\sqrt{2}\alpha}{\kappa T_2} \eta_L^* - \frac{\ell_0}{2} \mathcal{E}_L \quad (16)$$

where $\kappa = 2d/\hbar$, $\alpha = N\omega T_2 d^2 \sqrt{\mu/\epsilon}/\hbar$ is the Beer absorption coefficient of the material, and $\Delta = \omega_{ba} - \omega$ is the detuning of the field from the atomic resonance frequency. The loss term ℓ_0 has been added to the field equation heuristically, and in this context it represents only the waveguide loss.

We solve for the single-mode solution by setting the time-derivatives to zero and the slowly-varying envelope functions to be constants. In doing so, we are now making the distributed loss approximation because we are not allowing the fields to grow in space. Thus, ℓ_0 must now be taken to be the total loss, waveguide plus mirror loss. We take $\Delta = 0$ for simplicity, because the single-mode will lase very close to the peak of the gain spectrum. We denote the steady-state field amplitudes by $\mathcal{E}_R = \mathcal{E}_L = \mathcal{E}_0$ and find the LI curve

$$|\tilde{\mathcal{E}}_0|^2 = \frac{p-1}{1+\gamma_D/2} \quad (17)$$

where $\gamma_D = (1 + 4k^2 D T_1)^{-1}$ is the diffusion parameter. The steady-state population $w_0(z)$ is given by

$$w_0(z) = w_{th} \left[1 + \frac{\gamma_D}{2} \frac{p-1}{1+\gamma_D/2} - \gamma_D \frac{p-1}{1+\gamma_D/2} \cos(2k_0 z) \right]. \quad (18)$$

V. THEORY: POPULATION PULSATIONS

This section gives a more detailed derivation of the population pulsations, and demonstrates how to include nonzero detuning Δ and GVD into the formalism.

We begin by imagining a small volume of dipoles subject to a spatially uniform E -field to develop an understanding of the non-linear effects caused by the Bloch dynamics. The

electric field is given by

$$E(t) = \mathcal{E}(t)e^{i\omega t} + c.c. \quad (19)$$

The Bloch equations in the rotating wave approximation are

$$\dot{\sigma} = \left(i\Delta - \frac{1}{T_2}\right)\sigma + \frac{i\kappa}{2}w\mathcal{E} \quad (20)$$

$$\dot{w} = i\kappa(\mathcal{E}^*\sigma - \mathcal{E}\sigma^*) - \frac{w - w_{eq}}{T_1} \quad (21)$$

where σ is the off-diagonal element of the density matrix in the rotating frame, w is the population inversion (positive when inverted), $\Delta = \omega_{ba} - \omega$ is the detuning between the applied field and the resonant frequency of the two-level system, T_1 is the (longitudinal) population relaxation time, T_2 is the (transverse) dephasing time, $\kappa \equiv 2d/\hbar$ is the coupling constant where d is the dipole matrix element (assumed to be real) and \hbar is Planck's constant, and w_{eq} is the equilibrium population inversion in the absence of any electric field which is determined by the pumping. (Note that these equations are identical to Eqs. 3.19(a)-(c) in [1], except that we have allowed \mathcal{E} to be complex and left the off-diagonal component of the density matrix in complex notation rather than writing $\sigma = (u + iv)/2$.) With these conventions, the macroscopic polarization P (dipole moment per volume) in a region with a volume density of N dipoles is given by

$$P(t) = Nd\sigma e^{i\omega t} + c.c. \quad (22)$$

First, we consider the effect of a monochromatic field at frequency ω , obtained from Eqs. 20-21 by setting $\mathcal{E}(t) = \mathcal{E}_0$ and all time derivatives to zero. The result is a steady-state polarization σ_0 and population inversion w_0 given by

$$\sigma_0 = \frac{i\kappa T_2}{2(1 - i\Delta T_2)}w_0\mathcal{E}_0 \quad (23)$$

$$w_0 = \frac{w_{eq}}{1 + \frac{\kappa^2 T_1 T_2 |\mathcal{E}_0|^2}{1 + (\Delta T_2)^2}} \quad (24)$$

Note that the population inversion w_0 is saturated as the field strength \mathcal{E}_0 increases: this is responsible for saturable loss (when $w_{eq} < 0$) and saturable gain (when $w_{eq} > 0$).

A. Two-frequency operation

Next, we consider the E -field

$$\mathcal{E} = \mathcal{E}_0 + \mathcal{E}_+ e^{i\delta\omega t} \quad (25)$$

which consists of the strong field \mathcal{E}_0 at frequency ω superposed with the much weaker field \mathcal{E}_+ detuned from ω by $\delta\omega$. A polarization will of course be induced at $\omega + \delta\omega$. However, a polarization at $\omega - \delta\omega$ also results due to the beat note at $\delta\omega$ which modulates the intensity: the resulting modulation of the population inversion with time (i.e., a population pulsation) leads to nonlinear frequency mixing. We express the full polarization as

$$P(t) = \sum_{m=-,0,+} \mathcal{P}_m e^{i\omega_m t} + c.c. \quad (26)$$

where $\omega_+ \equiv \omega + \delta\omega$ and $\omega_- \equiv \omega - \delta\omega$. We can solve for the polarization as done in [3], keeping only terms to first order in the weak field \mathcal{E}_+ , which gives

$$\mathcal{P}_0 = \frac{i\epsilon}{\omega_{ba}} \bar{\alpha} w_0 \frac{\mathcal{E}_0}{1 - i\Delta T_2} \quad (27)$$

$$\mathcal{P}_+ = \frac{i\epsilon}{\omega_{ba}} \bar{\alpha} w_0 \left[\frac{\mathcal{E}_+}{1 - i(\Delta - \delta\omega)T_2} + \Lambda_+^+ \tilde{\mathcal{E}}_0 \tilde{\mathcal{E}}_0^* \mathcal{E}_+ \right] \quad (28)$$

$$\mathcal{P}_- = \frac{i\epsilon}{\omega_{ba}} \bar{\alpha} w_0 \Lambda_-^+ \tilde{\mathcal{E}}_0 \tilde{\mathcal{E}}_0^* \mathcal{E}_+ \quad (29)$$

where

$$\Lambda_+^+ = \frac{-[1 + i(\Delta + \delta\omega)T_2](1 + i\delta\omega T_2/2)}{[1 - i(\Delta - \delta\omega)T_2](1 + i\Delta T_2) \left[(1 + i\delta\omega T_1)[1 + i(\Delta + \delta\omega)T_2][1 - i(\Delta - \delta\omega)T_2] + (1 + i\delta\omega T_2)|\tilde{\mathcal{E}}_0|^2 \right]} \quad (30)$$

$$\Lambda_-^+ = \frac{-(1 - i\delta\omega T_2/2)}{(1 - i\Delta T_2) \left[(1 - i\delta\omega T_1)[1 + i(\Delta - \delta\omega)T_2][1 - i(\Delta + \delta\omega)T_2] + (1 - i\delta\omega T_2)|\tilde{\mathcal{E}}_0|^2 \right]} \quad (31)$$

are the self-mixing and cross-mixing coupling coefficients, respectively. We consider the dipoles to be embedded in a host medium of permittivity ϵ and permeability μ . (We adopt the convention of [4]: ϵ , μ and the speed of light $c = 1/\sqrt{\epsilon\mu}$ always take their values in the background host medium.) Many of the material properties of the two-level system are lumped into the ‘‘Beer loss rate’’

$$\bar{\alpha} = \frac{Nd^2 T_2 \omega_{ba} c \sqrt{\mu/\epsilon}}{\hbar}, \quad (32)$$

which is related to the more familiar Beer absorption coefficient α (with units of inverse length) that appears in Beers law of absorption by $\bar{\alpha} = \alpha c$. (Note, however, that in our expressions for the polarization due to the two-level system, all factors of ϵ and μ drop

out; that is, these expressions do not contain the polarization contributions due to the background medium.) The central mode amplitude \mathcal{E}_0 has been normalized such that $\tilde{\mathcal{E}}_0 \equiv \kappa\sqrt{T_1 T_2}\mathcal{E}_0$. Note that \mathcal{P}_0 is unaffected to first order in \mathcal{E}_+ . The polarization \mathcal{P}_+ comes from two contributions. First, there is the linear contribution from the Lorentz oscillator which \mathcal{E}_+ would induce even in the absence of the strong field \mathcal{E}_0 . Second, there is a contribution due to the PP which is described by the term Λ_+^+ . The term \mathcal{P}_- is due solely to the PP and is governed by Λ_-^+ . Note that the full polarization is directly proportional to the steady-state population inversion w_0 ; this will be important when we generalize our results to standing-wave cavities, where w_0 varies with position.

Now that we have the polarization, we can calculate the gain seen by the sideband field. We define the gain \bar{g} (with dimension of frequency) of the sideband as the power density generated at $\omega + \delta\omega$ by the interaction of the field with the dipoles—considering only field and polarization terms oscillating at $\omega + \delta\omega$ —divided by the energy density of the exciting sideband field, or

$$\bar{g}_+ \equiv -\frac{\langle E\dot{P} \rangle_+}{2\epsilon|\mathcal{E}_+|^2} \quad (33)$$

$$= \frac{i\omega_+(\mathcal{E}_+\mathcal{P}_+^* - \mathcal{E}_+^*\mathcal{P}_+)}{2\epsilon|\mathcal{E}_+|^2} \quad (34)$$

1. $\Delta = 0$

Here we consider the case of zero detuning, $\Delta = 0$, which simplifies the mathematical expressions considerably and is a prerequisite to understanding the case of non-zero detuning. Under this simplified scenario, we denote the self-mixing coefficient Λ_+^+ by Λ , where

$$\Lambda = \frac{-(1 + i\delta\omega T_2/2)}{\left[(1 + i\delta\omega T_1)(1 + i\delta\omega T_2)^2 + (1 + i\delta\omega T_2)|\tilde{\mathcal{E}}_0|^2\right]}, \quad (35)$$

and it is simple to show that the cross-coupling coefficient Λ_-^+ is simply Λ^* . The gain of the sideband field is found to be

$$\bar{g}_+ = \bar{\alpha}w_0 \left[\frac{1}{1 + (\delta\omega T_2)^2} + \text{Real}(\Lambda)|\tilde{\mathcal{E}}_0|^2 \right]. \quad (36)$$

(We have used $(\omega + \delta\omega)/\omega_{ba} \approx 1$.) Thus, the gain can be nicely divided up into a contribution from the Lorentz oscillator and a contribution from the PP. All of this is proportional to $\bar{\alpha}w_0$: $\bar{\alpha}$ gives you the gain of a weak field tuned to line-center in a perfectly inverted medium

(or alternatively, the loss seen by a weak field tuned to line-center in a material in its ground state), and w_0 gives you the expectation value of finding an electron in the excited state (equal to 1 when excited, -1 when in the ground state, and 0 at transparency). Note that $\text{Real}(\Lambda)$ can be positive or negative, which we will discuss shortly.

B. Three-frequency operation

Of course, the polarization created at $\omega - \delta\omega$ will create a field at that frequency, which is precisely why in the experiments we always observe the two sidebands appearing simultaneously. One sideband cannot exist in isolation when the mixing terms naturally couple them together. Therefore, we need to consider the field

$$\mathcal{E} = \mathcal{E}_0 + \mathcal{E}_+ e^{i\delta\omega t} + \mathcal{E}_- e^{-i\delta\omega t}. \quad (37)$$

The polarization at each sideband frequency now contains a Lorentzian term, a self-mixing term, and a cross-mixing term:

$$\mathcal{P}_+ = \frac{i\epsilon}{\omega_{ba}} \bar{\alpha} w_0 \left[\frac{\mathcal{E}_+}{[1 - i(\Delta - \delta\omega)T_2]} + \Lambda_+^+ \tilde{\mathcal{E}}_0 \tilde{\mathcal{E}}_0^* \mathcal{E}_+ + \Lambda_+^- \tilde{\mathcal{E}}_0 \tilde{\mathcal{E}}_0^* \mathcal{E}_-^* \right] \quad (38)$$

$$\mathcal{P}_- = \frac{i\epsilon}{\omega_{ba}} \bar{\alpha} w_0 \left[\frac{\mathcal{E}_-}{[1 - i(\Delta + \delta\omega)T_2]} + \Lambda_-^- \tilde{\mathcal{E}}_0 \tilde{\mathcal{E}}_0^* \mathcal{E}_- + \Lambda_-^+ \tilde{\mathcal{E}}_0 \tilde{\mathcal{E}}_0^* \mathcal{E}_+^* \right] \quad (39)$$

where Λ_-^- and Λ_+^- are obtained by making the substitution $\delta\omega \rightarrow -\delta\omega$ in the expressions for Λ_+^+ and Λ_-^+ , respectively, given in Eqs. 30-31 .

1. $\Delta = 0$

Let us again focus on the case $\Delta = 0$, for which the polarization at each sideband simplifies to

$$\mathcal{P}_+ = \frac{i\epsilon}{\omega_{ba}} \bar{\alpha} w_0 \left[\frac{\mathcal{E}_+}{[1 + i\delta\omega T_2]} + \Lambda \tilde{\mathcal{E}}_0 \tilde{\mathcal{E}}_0^* \mathcal{E}_+ + \Lambda \tilde{\mathcal{E}}_0 \tilde{\mathcal{E}}_0^* \mathcal{E}_-^* \right] \quad (40)$$

$$\mathcal{P}_- = \frac{i\epsilon}{\omega_{ba}} \bar{\alpha} w_0 \left[\frac{\mathcal{E}_-}{[1 - i\delta\omega T_2]} + \Lambda^* \tilde{\mathcal{E}}_0 \tilde{\mathcal{E}}_0^* \mathcal{E}_- + \Lambda^* \tilde{\mathcal{E}}_0 \tilde{\mathcal{E}}_0^* \mathcal{E}_+^* \right], \quad (41)$$

where Λ is simply Λ_+^+ evaluated for $\Delta = 0$. We see the nice property that when $\Delta = 0$, $\Lambda_+^+ = \Lambda_+^-$ ($\equiv \Lambda$), and $\Lambda_-^- = \Lambda_-^+$ ($\equiv \Lambda^*$); in other words, the self- and cross-mixing coupling coefficients are equal.

The gain \bar{g}_+ of the positive sideband is

$$\bar{g}_+ = \bar{\alpha}w_0 \left\{ \frac{1}{1 + (\delta\omega T_2)^2} + \text{Real} \left[\Lambda |\tilde{\mathcal{E}}_0|^2 \left(1 + \frac{\tilde{\mathcal{E}}_0^2 \mathcal{E}_-^*}{|\tilde{\mathcal{E}}_0|^2 \mathcal{E}_+} \right) \right] \right\}, \quad (42)$$

and a similar expression holds for the minus sideband. This equation tells us that the PP contribution to the gain depends on the phase and amplitude relationships of \mathcal{E}_0 , \mathcal{E}_- , and \mathcal{E}_+ , which is not too surprising because the amplitude of the PP itself is sensitive to these parameters. Without loss of generality, we can take \mathcal{E}_0 to be real. If $\mathcal{E}_+ = \mathcal{E}_-^*$, then the two sidebands' contributions to the beat note at $\delta\omega$ add constructively, resulting in a field whose amplitude modulation (AM) is twice the strength of a field with only one sideband. If $\mathcal{E}_+ = -\mathcal{E}_-^*$, then the two sidebands' contributions to the beat note at $\delta\omega$ destructively cancel and there is no longer any amplitude modulation at frequency $\delta\omega$. We refer to such a field as frequency-modulated (FM). We see from Eq. 42 that the AM sidebands therefore experience a PP contribution to the gain that is twice as large as the single sideband case, while the FM sidebands experiences only the background Lorentzian gain, consistent with the fact that there is no PP in this case. We summarize this with the formula for the gain \bar{g} of each sideband for the case of equal-amplitude sidebands ($|\mathcal{E}_+| = |\mathcal{E}_-|$),

$$\bar{g} = \bar{\alpha}w_0 \left[\frac{1}{1 + (\delta\omega T_2)^2} + \text{Real}(\Lambda) |\tilde{\mathcal{E}}_0|^2 \begin{cases} 2 & ; \text{AM} \\ 0 & ; \text{FM} \end{cases} \right]. \quad (43)$$

Note that for a superposition of AM and FM, the gain due to the PP will fall between 0 and 2 times the factor $\text{Real}(\Lambda) |\tilde{\mathcal{E}}_0|^2$.

VI. THEORY: INSTABILITY THRESHOLD

This section gives a more detailed derivation of the instability threshold, combining the populating grating and the population pulsations into.

When a continuous-wave (cw) laser is pumped at its lasing threshold, only a single frequency of light—the one nearest the gain peak that also satisfies the roundtrip phase condition—has sufficient gain to overcome the roundtrip loss and begins to lase. As the pumping is increased, the single-mode solution yields to multimode operation; this is known as the single-mode instability. Our goal is to determine 1) how hard to pump the laser to reach the single-mode instability and 2) which new frequencies start lasing.

Consider a laser pumped above threshold that is lasing on a single-mode, which we refer to as the primary or central mode. If another mode is to lase, it must be seeded by a spontaneously generated photon at a different frequency. This photon will necessarily create a beat note through its coexistence with the primary mode, resulting in a population pulsation. The gain seen by the new frequency must therefore account for this parametric gain in addition to the background Lorentzian gain. Furthermore, the PP couples the sideband to the symmetrically detuned sideband frequency on the other side of the primary mode, so we should in general assume the presence of both sidebands. Because the instability threshold depends on the cavity geometry, we will consider a traveling-wave laser as well as a standing-wave laser. In both cases, the strategy is the same. First, we solve for the single-mode intensity \mathcal{E}_0 and the population inversion $w_0(z)$ as a function of the pumping, entirely neglecting the sidebands. Knowing this, we can then calculate the sideband gain in the presence of the primary mode.

We start with the wave equation

$$\frac{\partial^2 E}{\partial z^2} - \frac{1}{c^2} \frac{\partial^2 E}{\partial t^2} = \mu \frac{\partial^2 P}{\partial t^2}. \quad (44)$$

Following the approach used to calculate the optical parametric oscillation threshold in optically pumped microresonators [5], we expand the field in terms of the cold cavity modes,

$$E(z, t) = \sum_{m=-,0,+} \mathcal{E}_m(t) \Upsilon_m(z) e^{i\omega_m t} + c.c. \quad (45)$$

The spatial modes obey the normalization condition

$$\frac{1}{L} \int_0^L dz |\Upsilon_m(z)|^2 = 1. \quad (46)$$

When group velocity dispersion (GVD) is non-zero, the two modes ω_+ and ω_- will not be equidistant from ω_0 . We have also assumed that the spatial and temporal dependence of the modes can be separated. This is a good approximation in the case of a laser, because we know the intracavity field will be sharply resonant at the modes. The spatial variation of the polarization can be described by making the substitution $\mathcal{E}_m \rightarrow \mathcal{E}_m \Upsilon_m(z)$ and $w_0 \rightarrow w_0(z)$ into the polarization Eqs. 38-39, which results in the polarization

$$P(z, t) = \sum_{m=-,0,+} \mathcal{P}_m(z, t) e^{i\omega_m t} + c.c. \quad (47)$$

where

$$\mathcal{P}_+(z, t) = \frac{i\epsilon}{\omega_{ba}} \bar{\alpha} w_0(z) \left[\frac{\mathcal{E}_+ \Upsilon_+(z)}{[1 - i(\Delta - \delta\omega)T_2]} + \Lambda_+^+(z) |\Upsilon_0(z)|^2 \Upsilon_+(z) |\tilde{\mathcal{E}}_0|^2 \mathcal{E}_+ + \Lambda_+^-(z) \Upsilon_0(z)^2 \Upsilon_-^*(z) e^{i\bar{\omega}t} \tilde{\mathcal{E}}_0^2 \mathcal{E}_-^* \right] \quad (48)$$

$$\mathcal{P}_-(z, t) = \frac{i\epsilon}{\omega_{ba}} \bar{\alpha} w_0(z) \left[\frac{\mathcal{E}_- \Upsilon_-(z)}{[1 - i(\Delta + \delta\omega)T_2]} + \Lambda_-^-(z) |\Upsilon_0(z)|^2 \Upsilon_-(z) |\tilde{\mathcal{E}}_0|^2 \mathcal{E}_- + \Lambda_-^+(z) \Upsilon_0(z)^2 \Upsilon_+^*(z) e^{i\bar{\omega}t} \tilde{\mathcal{E}}_0^2 \mathcal{E}_+^* \right]. \quad (49)$$

We have introduced $\bar{\omega} \equiv 2\omega_0 - \omega_+ - \omega_-$, the deviation of the cold cavity modes from equal spacing. Note that the Λ s now depend on z due to the term in their denominators dependent on the primary mode amplitude. Because we no longer demand that the two sidebands have the same detuning $\delta\omega$, Λ_+^+ and Λ_-^+ should, strictly speaking, be calculated using the detuning $\delta\omega_+ = \omega_+ - \omega_0$, while Λ_-^- and Λ_+^- should depend on $\delta\omega_- = \omega_0 - \omega_-$. In practice, we can ignore this difference in the Λ s; the term $e^{i\bar{\omega}t}$ captures the most important effect of GVD.

Plugging everything into the wave equation gives

$$\sum_m \left(\frac{d^2 \Upsilon_m}{dz^2} + \frac{\omega_m^2}{c^2} \Upsilon_m \right) \mathcal{E}_m e^{i\omega_m t} - \frac{2i}{c^2} \sum_m \omega_m \frac{d\mathcal{E}_m}{dt} \Upsilon_m e^{i\omega_m t} = \mu \sum_m -\omega_m^2 (\mathcal{P}_m - \mathcal{P}_{m,\text{loss}}) e^{i\omega_m t} \quad (50)$$

where the slowly-varying-envelope approximation allowed us to ignore second time derivatives of \mathcal{E}_m on the left-hand side, and first and second derivatives of \mathcal{E}_m on the right-hand side. The spatial modes $\Upsilon_m(z)$ are chosen so that the first term on the LHS equals zero. The loss of each mode has been added to the equation in the form of a polarization contribution; we assume each mode has the same linear loss, which can be expressed

$$\mathcal{P}_{m,\text{loss}}(z, t) = \frac{i\epsilon}{\omega_{ba}} \bar{\ell} \Upsilon_m(z) \mathcal{E}_m(t). \quad (51)$$

Equation 50 couples all of the modes \mathcal{E}_m . We can project this equation onto each mode by multiplying by $\Upsilon_n(z)$ and integrating over the length of the laser cavity, thus taking advantage of the orthonormality of the spatial modes $\Upsilon_m(z)$, and then equating terms which oscillate at the same frequency (since terms with different frequencies will not affect the time-averaged gain seen by a mode). The result is one equation for the central mode

$$\dot{\mathcal{E}}_0 = \left[-\frac{\bar{\ell}}{2} + \frac{\bar{\alpha}}{2(1 - i\Delta T_2)} \int \frac{dz}{L} w_0(z) |\Upsilon_0(z)|^2 \right] \mathcal{E}_0, \quad (52)$$

one for the positive sideband

$$\begin{aligned}\dot{\mathcal{E}}_+ = & -\frac{\bar{\ell}}{2}\mathcal{E}_+ + \frac{\bar{\alpha}}{2} \left[\frac{\mathcal{E}_+}{1-i(\Delta-\delta\omega)T_2} \int \frac{dz}{L} w_0(z)|\Upsilon_+(z)|^2 \right. \\ & + |\tilde{\mathcal{E}}_0|^2 \mathcal{E}_+ \int \frac{dz}{L} w_0(z)\Lambda_+^+(z)|\Upsilon_0(z)|^2|\Upsilon_+(z)|^2 \\ & \left. + \tilde{\mathcal{E}}_0^2 \mathcal{E}_+^* e^{i\bar{\omega}t} \int \frac{dz}{L} w_0(z)\Lambda_+^-(z)\Upsilon_0(z)^2\Upsilon_-^*(z)\Upsilon_+(z) \right],\end{aligned}\quad (53)$$

and one for the negative sideband

$$\begin{aligned}\dot{\mathcal{E}}_- = & -\frac{\bar{\ell}}{2}\mathcal{E}_- + \frac{\bar{\alpha}}{2} \left[\frac{\mathcal{E}_-}{1-i(\Delta+\delta\omega)T_2} \int \frac{dz}{L} w_0(z)|\Upsilon_-(z)|^2 \right. \\ & + |\tilde{\mathcal{E}}_0|^2 \mathcal{E}_- \int \frac{dz}{L} w_0(z)\Lambda_-^-(z)|\Upsilon_0(z)|^2|\Upsilon_-(z)|^2 \\ & \left. + \tilde{\mathcal{E}}_0^2 \mathcal{E}_-^* e^{i\bar{\omega}t} \int \frac{dz}{L} w_0(z)\Lambda_-^+(z)\Upsilon_0(z)^2\Upsilon_+^*(z)\Upsilon_-(z) \right].\end{aligned}\quad (54)$$

These three equations will be used to understand the instability threshold. In general, one must first apply the steady-state condition $\dot{\mathcal{E}}_0 = 0$ to Eq. 52 which, together with the Bloch equation relating the field to the inversion, will yield the amplitude of the primary mode \mathcal{E}_0 along with the resulting population inversion $w_0(z)$, both as a function of the pumping w_{eq} . This information is then used in Eqs. 53-54 to determine the minimum level of pumping w_{eq} at which a pair of sidebands with detuning $\delta\omega$ experiences more gain than loss. This is the instability threshold.

So far, we have kept Eqs. 52-54 as general as possible to account for arbitrary spatial profiles, GVD, and detuning Δ between the lasing mode and the peak of the gain spectrum. From here on we will simplify the problem by taking $\bar{\omega} = 0$ (zero GVD) and $\Delta = 0$, and apply these conditions to the simplest possible traveling-wave and standing-wave cavities.

A. Traveling-wave cavity

For the traveling-wave laser, the spatial modes are

$$\Upsilon_m(z) = e^{-ik_m z} \quad (55)$$

so every point in the cavity sees the same intensity. At and above threshold, the population inversion is everywhere saturated to the threshold inversion, so w_0 is independent of z . For $\Delta = 0$, the inversion is

$$w_0 = w_{th} \equiv \frac{\bar{\ell}}{\bar{\alpha}} \quad (56)$$

and the intensity of the primary mode is given by

$$|\tilde{\mathcal{E}}_0|^2 = p - 1 \quad (57)$$

where we have made use of the normalized primary mode amplitude $\tilde{\mathcal{E}}_0 \equiv \kappa\sqrt{T_1 T_2} \mathcal{E}_0$, and p is the pumping parameter defined as $p \equiv w_{eq}/w_{th}$. Because $|\tilde{\mathcal{E}}_0|^2$ is independent of z , all of the Λ s are independent of z . Furthermore, since both w_0 and the Λ s are independent of z , they can be pulled out of the spatial integrals in Eqs. 53-54. These integrals are then equal to one, where we have used the zero GVD condition $\bar{\omega} = 0$ in order for the cross-overlap integral (the last integral in each equation) to equal one. The sideband equations become

$$\dot{\mathcal{E}}_+ = -\frac{\bar{\ell}}{2}\mathcal{E}_+ + \frac{\bar{\alpha}w_{th}}{2} \left[\frac{\mathcal{E}_+}{1+i\delta\omega T_2} + \Lambda|\tilde{\mathcal{E}}_0|^2\mathcal{E}_+ + \Lambda\tilde{\mathcal{E}}_0^2\mathcal{E}_-^* \right] \quad (58)$$

$$\dot{\mathcal{E}}_- = -\frac{\bar{\ell}}{2}\mathcal{E}_- + \frac{\bar{\alpha}w_{th}}{2} \left[\frac{\mathcal{E}_-}{1-i\delta\omega T_2} + \Lambda^*|\tilde{\mathcal{E}}_0|^2\mathcal{E}_- + \Lambda^*\tilde{\mathcal{E}}_0^2\mathcal{E}_+^* \right] \quad (59)$$

which can be written in matrix form

$$\begin{pmatrix} \dot{\mathcal{E}}_+ \\ \dot{\mathcal{E}}_-^* \end{pmatrix} = \begin{pmatrix} M_+ & R_+ \\ R_-^* & M_-^* \end{pmatrix} \begin{pmatrix} \mathcal{E}_+ \\ \mathcal{E}_-^* \end{pmatrix} \quad (60)$$

where

$$M_+ = M_-^* = -\frac{\bar{\ell}}{2} + \frac{\bar{\alpha}w_{th}}{2} \left(\frac{1}{1+i\delta\omega T_2} + \Lambda|\tilde{\mathcal{E}}_0|^2 \right) \quad (61)$$

$$R_+ = R_-^* = \frac{\bar{\alpha}w_{th}}{2} \Lambda|\tilde{\mathcal{E}}_0|^2. \quad (62)$$

(In the last step, we have finally taken the freedom to choose $\tilde{\mathcal{E}}_0$ to be real, which we can do at this point without loss of generality.)

Now, if we assume a solution of the form $\mathcal{E}_{\pm} \sim e^{\lambda t}$, we find the two solutions for λ

$$\lambda = \frac{1}{2}[M_+ + M_-^* \pm \sqrt{(M_+ - M_-^*)^2 + 4R_+R_-^*}]. \quad (63)$$

The net gain seen by each sideband is given by $\text{Real}(2\lambda)$ (the factor of two is for intensity gain rather than amplitude gain), which includes the gain minus the loss. Subtracting off the loss, the gain \bar{g} seen by each sideband is

$$\bar{g} = \bar{\alpha}w_{th} \left[\frac{1}{1+(\delta\omega T_2)^2} + \begin{cases} 2 \text{ Real}(\Lambda)|\tilde{\mathcal{E}}_0|^2 & ; \text{ AM} \\ 0 & ; \text{ FM} \end{cases} \right] \quad (64)$$

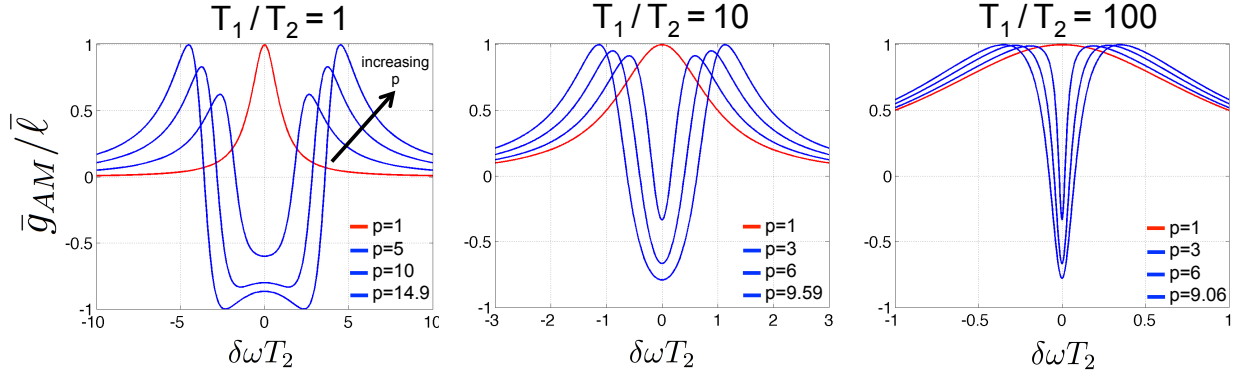


FIG. S5. The sideband gain $\bar{g}_{AM}/\bar{\ell}$ of a traveling-wave laser, given in Eq. 66, is plotted at various pump strengths, for three different values of Z : 1, 10, and 100. The largest value of p in each plot is equal to the instability threshold given in Eq. 69.

where the two solutions correspond to AM and FM sideband configurations. Finally, we recognize that the gain is pinned at threshold, so $\bar{\alpha}w_{th} = \bar{\ell}$, and we write down the sideband gain normalized to the loss

$$\frac{\bar{g}}{\bar{\ell}} = \frac{1}{1 + (\delta\omega T_2)^2} + \text{Real}(\Lambda)|\tilde{\mathcal{E}}_0|^2 \cdot \begin{cases} 2 & ; \text{AM} \\ 0 & ; \text{FM} \end{cases}. \quad (65)$$

When the gain \bar{g} exceeds the loss $\bar{\ell}$, the weak sideband amplitudes experience exponential growth, therefore the single-mode solution becomes unstable. Note that the Lorentzian term is always less than 1. This is a direct result of uniform gain clamping in the traveling-wave laser, which clamps the net gain of the mode at the peak of the Lorentzian to zero, and therefore any mode detuned from the peak will see slightly more loss than gain. FM sidebands therefore never become unstable because they only see the Lorentzian gain. On the other hand, AM sidebands induce a PP and with it a coherent gain term, which can provide enough extra gain on top of the Lorentzian background to allow the sidebands to lase,

$$\frac{\bar{g}_{AM}}{\bar{\ell}} = \frac{1}{1 + (\delta\omega T_2)^2} + 2 \text{Real}(\Lambda)|\tilde{\mathcal{E}}_0|^2. \quad (66)$$

To get a feel for the sideband gain, we have plotted $\bar{g}_{AM}/\bar{\ell}$ in Fig. S5 at various pump strengths p for $Z = 1, 10$, and 100 , where $Z \equiv T_1/T_2$. Graphically, we see that at large enough p sidebands will become unstable. Analytically, it is a simple matter to calculate

how hard to pump the laser p before the sidebands appear, starting from Eq. 66. We start by replacing $|\tilde{\mathcal{E}}_0|^2$ with $p - 1$, and note that this substitution must also be made in Λ , which implicitly varies with $|\tilde{\mathcal{E}}_0|^2$. Then, setting $\bar{g}_{AM}/\bar{\ell}$ equal to one, we can solve a simple quadratic formula for $\delta\omega^2$,

$$(\delta\omega T_2)^2 = \frac{-1 + 3Z(p - 1) \pm \sqrt{[1 - 3Z(p - 1)]^2 - 8Z^2p(p - 1)}}{2Z^2}. \quad (67)$$

Finally, we must apply some physical reasoning: as p is increased past 1, the sideband gain increases. Right at the moment when the instability threshold is reached, $\delta\omega^2$ must take on a single value. Thus, we set the radical in Eq. 67 to zero and solve for p . After solving another simple quadratic equation, we find that

$$p = 5 + \frac{3}{Z} \pm 4\sqrt{1 + \frac{3}{2Z} + \frac{1}{2Z^2}}. \quad (68)$$

How do we choose between the plus and minus sign? By plugging this expression for p back into Eq. 67, it is simple to check that only the plus sign yields real-valued solutions for $\delta\omega$. Thus, we have found the instability threshold, which we denote p_{RNGH} ,

$$p_{RNGH} = 5 + \frac{3}{Z} + 4\sqrt{1 + \frac{3}{2Z} + \frac{1}{2Z^2}} \quad (69)$$

because it is the well-known instability threshold found by Risken and Nummedal (see Eq. 3.10 in [6]) and Graham and Haken (see Eq. 7.35 in [7]). Plugging this value of p into Eq. 67 yields the value of $\delta\omega$ of the sidebands when the instability sets in

$$(\delta\omega_{RNGH} T_2)^2 = \frac{4}{Z^2} + \frac{6}{Z} \left(1 + \sqrt{1 + \frac{3}{2Z} + \frac{1}{2Z^2}} \right). \quad (70)$$

One thing to notice is that in the limit $Z \gg 1$ (transverse relaxation must faster than longitudinal relaxation), the instability threshold $p_{RNGH} \rightarrow 9$ from above and $\delta\omega_{RNGH} T_2 \rightarrow \sqrt{12/Z}$.

B. Standing-Wave Cavity

As before, we restrict ourselves to the case $\Delta = 0$ and $\bar{\omega} = 0$. We will see that calculations for the standing-wave cavity are significantly more complicated than for the traveling-wave cavity. The spatial variation of the primary mode causes the inversion w_0 and the coupling

Λ to both depend on z , which makes the integrals more difficult to compute. For this reason, we treat the problem to first order in the primary mode intensity $|\tilde{\mathcal{E}}_0|^2$, which allows us to compute the integrals analytically. However, the theory can be extended to higher order at will, or the integrals can always be computed numerically.

For the standing-wave laser with perfectly reflecting end mirrors, the spatial profile of each mode is given by

$$\Upsilon_m(z) = \sqrt{2} \cos(k_m z). \quad (71)$$

The spatial modulation of the intensity is responsible for the spatial modulation of the population inversion $w_0(z)$, though mitigated somewhat by carrier diffusion. We calculated $w_0(z)$ in Sec. IV of the supplementary information. The result is

$$w_0(z) = w_{th} \left[1 + \frac{\gamma_D}{2} \frac{p-1}{1+\gamma_D/2} - \gamma_D \frac{p-1}{1+\gamma_D/2} \cos(2k_0 z) \right]. \quad (72)$$

to first order in $|\tilde{\mathcal{E}}_0|^2$, where $w_{th} = \bar{\ell}/\bar{\alpha}$, and $\gamma_D = (1 + 4k^2 D T_1)^{-1}$ is the diffusion parameter. The spatial variation of the inversion has important consequences. For one, it reduces the power of the laser, which is given by

$$|\tilde{\mathcal{E}}_0|^2 = \frac{p-1}{1+\gamma_D/2}. \quad (73)$$

Secondly, the gain is no longer uniformly clamped by the primary lasing mode, which will allow new modes to lase even in the absence of PPs.

The spatial variation of the primary lasing mode also causes Λ to vary with position. In keeping with our approximations, we can expand Λ to zeroth order in $|\tilde{\mathcal{E}}_0|^2$ because in our equations Λ always multiplies $|\tilde{\mathcal{E}}_0|^2$, so the final result is first order in $|\tilde{\mathcal{E}}_0|^2$. We define the zeroth order expansion of Λ to be

$$\chi^{(3)} = \frac{-(1 + i\delta\omega T_2/2)}{(1 + i\delta\omega T_1)(1 + i\delta\omega T_2)^2}, \quad (74)$$

where the symbol $\chi^{(3)}$ was chosen to emphasize that this term now plays the role of a third-order nonlinear coefficient.

We start with the sideband Eqs. 53-54, replace $w_0(z)$ with Eq. 18, $\Lambda(z)$ with $\chi^{(3)}$, and keep only terms to first order in $|\tilde{\mathcal{E}}_0|^2$. The resulting equation for the growth of the positive

sideband is

$$\begin{aligned}\dot{\mathcal{E}}_+ = & -\frac{\bar{\ell}}{2}\mathcal{E}_+ + \frac{\bar{\alpha}w_{th}}{2} \left[\frac{1 + \frac{\gamma_D}{2}|\tilde{\mathcal{E}}_0|^2}{1 + i\delta\omega T_2} \mathcal{E}_+ \right. \\ & + \chi^{(3)}|\tilde{\mathcal{E}}_0|^2\mathcal{E}_+ \int \frac{dz}{L} |\Upsilon_0(z)|^2|\Upsilon_+(z)|^2 \\ & \left. + \chi^{(3)}\tilde{\mathcal{E}}_0^2\mathcal{E}_-^* \int \frac{dz}{L} \Upsilon_0(z)^2\Upsilon_-^*(z)\Upsilon_+^*(z) \right],\end{aligned}\quad (75)$$

and a similar equation can be written down for $\dot{\mathcal{E}}_-$. We define the longitudinal overlap integrals

$$\Gamma_{\text{self}} = \int_0^L \frac{dz}{L} |\Upsilon_0(z)|^2 |\Upsilon_+(z)|^2 = 1 \quad (76)$$

$$\Gamma_{\text{cross}} = \int_0^L \frac{dz}{L} \Upsilon_0(z)^2 \Upsilon_-^*(z) \Upsilon_+^*(z) = 1/2. \quad (77)$$

The implication is that the self-mixing interaction of a sideband with itself, mediated by the primary mode intensity, is twice as large as the cross-mixing interaction of one sideband generating gain for the other sideband, again mediated by the primary mode intensity. This is true only for the cosine-shaped modes that we have assumed, and the overlap integrals will change when the longitudinal spatial profile changes, as when the non-unity reflectivity of the facets is taken into account. The sideband Eqs. 53-54 become

$$\dot{\mathcal{E}}_+ = -\frac{\bar{\ell}}{2}\mathcal{E}_+ + \frac{\bar{\alpha}w_{th}}{2} \left[\frac{1 + \frac{\gamma_D}{2}|\tilde{\mathcal{E}}_0|^2}{1 + i\delta\omega T_2} \mathcal{E}_+ + \Gamma_{\text{self}}\chi^{(3)}|\tilde{\mathcal{E}}_0|^2\mathcal{E}_+ + \Gamma_{\text{cross}}\chi^{(3)}\tilde{\mathcal{E}}_0^2\mathcal{E}_-^* \right] \quad (78)$$

$$\dot{\mathcal{E}}_- = -\frac{\bar{\ell}}{2}\mathcal{E}_- + \frac{\bar{\alpha}w_{th}}{2} \left[\frac{1 + \frac{\gamma_D}{2}|\tilde{\mathcal{E}}_0|^2}{1 - i\delta\omega T_2} \mathcal{E}_- + \Gamma_{\text{self}}\chi^{(3)*}|\tilde{\mathcal{E}}_0|^2\mathcal{E}_- + \Gamma_{\text{cross}}\chi^{(3)*}\tilde{\mathcal{E}}_0^2\mathcal{E}_+^* \right], \quad (79)$$

which we express as

$$\begin{pmatrix} \dot{\mathcal{E}}_+ \\ \dot{\mathcal{E}}_-^* \end{pmatrix} = \begin{pmatrix} M_+ & R_+ \\ R_-^* & M_-^* \end{pmatrix} \begin{pmatrix} \mathcal{E}_+ \\ \mathcal{E}_-^* \end{pmatrix} \quad (80)$$

where

$$M_+ = M_-^* = -\frac{\bar{\ell}}{2} + \frac{\bar{\alpha}w_{th}}{2} \left(\frac{1 + \frac{\gamma_D}{2}|\tilde{\mathcal{E}}_0|^2}{1 + i\delta\omega T_2} + \Gamma_{\text{self}}\chi^{(3)}|\tilde{\mathcal{E}}_0|^2 \right) \quad (81)$$

$$R_+ = R_-^* = \frac{\bar{\alpha}w_{th}}{2} (\Gamma_{\text{cross}}\chi^{(3)}|\tilde{\mathcal{E}}_0|^2). \quad (82)$$

As we did for the traveling-wave laser, the sideband gain is easily calculated from these two coupled first-order differential equations. Normalizing the gain to the total loss, we find

$$\frac{\bar{g}}{\bar{\ell}} = \frac{1 + \frac{\gamma_D}{2}|\tilde{\mathcal{E}}_0|^2}{1 + (\delta\omega T_2)^2} + \text{Real}[\chi^{(3)}]|\tilde{\mathcal{E}}_0|^2 \cdot \begin{cases} \Gamma_{\text{self}} + \Gamma_{\text{cross}} = \frac{3}{2} & ; \text{AM} \\ \Gamma_{\text{self}} - \Gamma_{\text{cross}} = \frac{1}{2} & ; \text{FM} \end{cases}. \quad (83)$$

There are two things to notice here. As the laser pumping is increased, the term $\gamma_D |\tilde{\mathcal{E}}_0|^2/2$ grows, and consequently the gain is not clamped at the threshold value. This is due to spatial hole burning, or more precisely, the imperfect overlap of the standing-wave modes together with a finite amount of carrier diffusion. We view this background gain as a Lorentzian-shape whose amplitude increases with the pumping, and is therefore fully capable of pulling the sidebands above threshold, without any additional PP contribution to the gain.

Secondly, the PP contribution to the gain never vanishes. Even when the sidebands are phased such that an FM waveform is emitted from the laser, there is still a PP within the laser cavity. The reason for this is the imperfect overlap of the two sidebands' spatial modes, which means that at any given position within the cavity, the plus and minus sideband are likely to have different amplitudes. Therefore, even if the two sidebands are phased such that their contributions to the beat note at $\delta\omega$ destructively interfere with each other, the destruction is not perfect. The amplitude of the PP varies with position in the cavity, and in locations where the two sideband amplitudes are equal the PP will not exist, but the spatially averaged effect of the FM PP yields the factor of 1/2 in Eq. 83. By the same token, sidebands phased for AM will not fully constructively interfere, yielding a factor of 3/2 for the PP contribution to the gain rather than the factor 2, as it would be for the traveling-wave laser.

VII. NUMERICALLY CALCULATING THE INSTABILITY THRESHOLD

In this section, we demonstrate the predictions of the theory for the three uncoated lasers, and compare the results with the measurements.

Because the theory assumes end mirrors with unity reflectivity, we can only expect Eq. 83 to apply reasonably well to the uncoated QCLs. For each device, γ_D is calculated using the theoretical value of T_{up} (calculated from the bandstructure) and the diffusion constant $D = 77 \text{ cm}^2/\text{s}$ [8], giving $\gamma_D = 0.4$ (DS-3.8), 0.49 (TL-4.6), and 0.93 (LL-9.8). For these large values of γ_D , the incoherent gain increases rapidly with the pumping, and we find from Eq. 83 that the FM instability will have a lower threshold than the AM instability, regardless of the value of T_1 . The gain recovery time T_1 of each QCL is not as easily calculable as T_{up} because it depends on a few other time constants of the active region, such as the escape time of the electron from one injector region to the next active region. Therefore, we treat T_1 as a

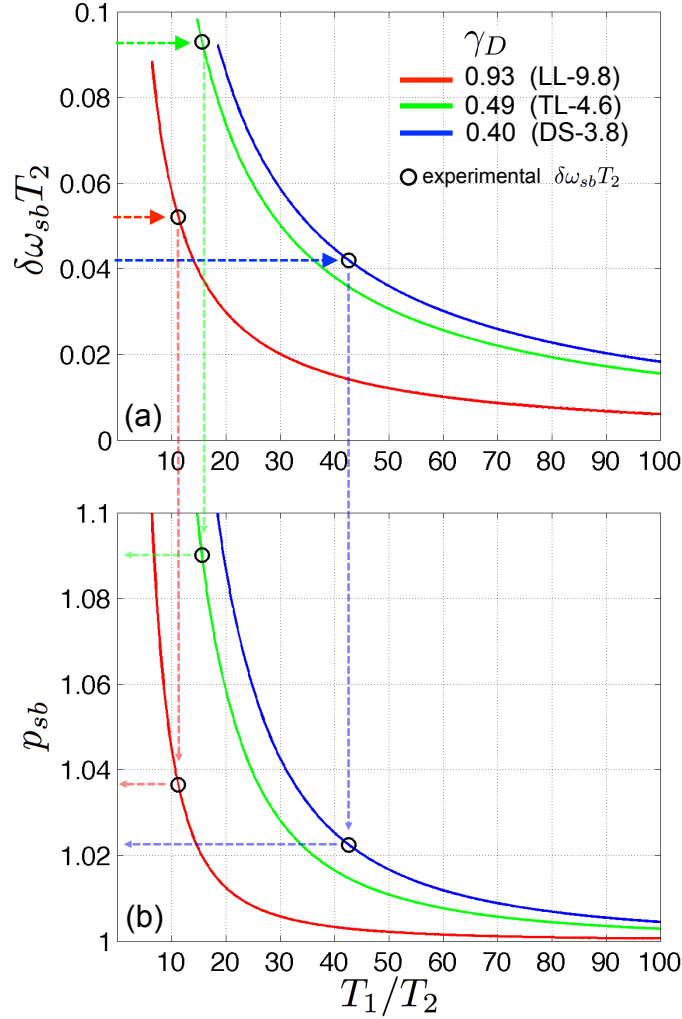


FIG. S6. Numerical solutions of the instability threshold obtained by setting the gain \bar{g} in Eq. 83 equal to the loss $\bar{\ell}$, yielding both (a) the sideband separation $\delta\omega_{sb}T_2$ and (b) the pumping p_{sb} . The experimentally measured values of $\delta\omega_{sb}T_2$ are compared to the theory to infer T_1/T_2 , which also gives the theoretical prediction for the instability threshold p_{sb} .

variable and calculate the instability threshold p_{sb} and sideband spacing $\delta\omega_{sb}$ as a function of T_1 . The resulting curves are shown in Fig. S6. By comparing the curves with the measured values of $\delta\omega_{sb}$, we can deduce the values $T_1 = 1.83$ ps (DS-3.8), 1.15 ps (TL-4.6), and 0.91 ps (LL-9.8). For these values of T_1 , the theory predicts an instability threshold of $p_{sb} = 1.02$ (DS-3.8), 1.09 (TL-4.6), and 1.04 (LL-9.8). It is encouraging that these fitted values of T_1 are close to the accepted value of the QCL gain recovery time, which has been shown by pump-probe experiments [9, 10] and theory [11] to be around 2 ps. However, the predicted

p_{sb} is significantly lower than the measured values $J_{\text{sb}}/J_{\text{th}} = 1.12$ (DS-3.8), 1.17 (TL-4.6), and 1.14 (LL-9.8), and the discrepancy is made worse by the fact that J/J_{th} is likely an underestimate of p (see the discussion in Sec. I of the supplement). The fact that the theory underestimates the instability threshold is perhaps not surprising, as we have only made sure that one of the two necessary conditions for sideband oscillation is satisfied (gain, not phase). We hope that future work which accounts for the detuning Δ , the detuning between the lasing mode and the cold cavity mode it occupies, and GVD can accurately predict the instability threshold, which would be a milestone in the understanding of lasers, and also yield a novel laser characterization method of lifetimes and diffusion rates by comparing measured values of p_{sb} and $\delta\omega_{\text{sb}}$ to an established theory.

-
- [1] L. Allen and J. Eberly, *Optical Resonance and Two-Level Atoms* (Dover Publications, New York, 1987).
 - [2] A. Gordon, C. Wang, L. Diehl, F. Kärtner, A. Belyanin, D. Bour, S. Corzine, G. Höfler, H. Liu, H. Schneider, T. Maier, M. Troccoli, J. Faist, and F. Capasso, *Phys. Rev. A* **77**, 053804 (2008).
 - [3] R. W. Boyd, *Nonlinear Optics*, 2nd ed. (Academic Press, San Diego, 2003).
 - [4] A. Siegman, *Lasers* (University Science Books, Sausalito, 1986) pp. 473–89.
 - [5] Y. K. Chembo and N. Yu, *Phys. Rev. A* **82**, 033801 (2010).
 - [6] H. Risken and K. Nummedal, *J. Appl. Phys.* **39**, 4662 (1968).
 - [7] R. Graham and H. Haken, *Zeitschrift für Phys.* **213**, 420 (1968).
 - [8] J. Faist, *Quantum Cascade Lasers*, 1st ed. (Oxford University Press, Oxford, 2013).
 - [9] H. Choi, L. Diehl, Z.-K. Wu, M. Giovannini, J. Faist, F. Capasso, and T. Norris, *Phys. Rev. Lett.* **100**, 167401 (2008).
 - [10] H. Choi, L. Diehl, Z.-K. Wu, M. Giovannini, J. Faist, F. Capasso, and T. B. Norris, *IEEE J. Quantum Electron.* **45**, 307 (2009).
 - [11] M. A. Talukder, *J. Appl. Phys.* **109**, 033104 (2011).